Journal of Ultrafine Grained and Nanostructured Materials
https://jufgnsm.ut.ac.ir
Vol. 51, No.2, December 2018, pp. 115-122
Print ISSN: 2423-6845 Online ISSN: 2423-6837
DOI: 10.22059/JUFGNSM.2018.02.03

Initial Discharge Capacity of Manganese Cobaltite as Anode Material for Lithium Ion Batteries

Mehrdad Dorri, Cyrus Zamani*, Alireza Babaei

School of Metallurgy and Materials Engineering, College of Engineering, University of Tehran, Tehran, Iran.

Recieved: 30 July 2018; Accepted: 8 September 2018

** Corresponding author email: c.zamani@ut.ac.ir*

ABSTRACT

Nanostructured manganese cobalt oxide spinel ($MnCo_2O_4$) are prepared by co-precipitation method and calcined at 650 and 750°C. Morphological studies show that by increasing the calcination temperature from 650 to 750°C, morphology of the particles changes from quasi-plate to polyhedral. The $MnCo_2O_4$ calcined at 650°C could deliver an initial discharge capacity of 1438 mAh g^{-1} under current density of 45 mA g^{-1}. The effects of calcination temperature on the initial discharge capacity of the electrode have also been investigated, The $MnCo_2O_4$ calcined at 650°C shows the higher initial discharge capacity due to the higher surface area (due to smaller particles) and weaker crystallinity. The influences of electrode porosities also have been studied, which suggest the electrochemical performance is determined by both the particle-to-particle contact and wettability of the electrode. An increase of the internal resistance of the electrode is observed with increasing electrode thickness (active material loading), which is the main factor responsible for the significant capacity loss for thicker electrode.

Keywords: *Lithium-ion battery; $MnCo_2O_4$; Electrode porosity; Transition metal oxide anode; Discharge capacity.*

1. Introduction

With the growth of electronic industry, energy storage is becoming an important issue. Rechargeable lithium-ion batteries (LIBs) are considered as unparalleled energy storage devices thanks to their high energy density, environmental benignity and long cycle life [1]. This kind of energy storage devices are used in a variety of technologies such as portable electronics [2], pure electric or hybrid electric vehicles [3], smart power grid [4] and so on [5].

Since their introduction to the market, graphite has been commonly used as the anode material in most industrial productions of LIBs, based on intercalation reaction [6]. Despite their several advantages, graphitic anodes present limited theoretical specific capacity of 372 mAh g^{-1} [7].

To cope with this limitation, conversion reaction-based oxide materials are fine alternatives for the intercalation reaction materials based on their high specific capacity [8]. Relatively high specific capacity, high metallurgical achievability, large resource stock, low cost, and environmental benignity makes transition metal oxide a unique candidate for anode materials among the other materials for the next-generation LIBs [9-12].

Co-based oxides ($CoCo_2O_4$) have attracted broad attention because of their high specific capacity (890 mAh g^{-1}). Previous reports show that several formidable challenges still remain. Easy agglomeration, intrinsically low conductivity of this material during charge and discharge process and high cost of Co-based oxides [13-16].

Efforts have been made to solve these disobedient problems, like nanostructuring [17, 18], doping [19], compositing [20-22] and forming compound

metal oxides [23].

Following this way, works have been conducted on the development of Co-based oxide anodes by partial substitution of Co by Zn [24], Cu [25], Fe [26], or other low-cost spinel oxides [27-30]. Embedding Manganese (Mn) to the A sites of the spinel oxides is an effective method to improve the electrochemical performance. Firstly because its abundance in nature lowers the cost of anode material. Secondly, cycling performance improves owing to high intrinsic conductivity caused by the introduction of Mn while the operation voltage of Co_3O_4 is decreased [31]. Kim and co-workers reported the synthesis of hollow nanofibers via the electrospinning, the initial discharge capacity of which was measured to be 1402 mAh g^{-1} at a current density of 100 mA g^{-1}. The reported device could retain a reversible discharge capacity of 997 mAh g^{-1} after 50 cycles [32]. Li and co-workers also synthesized hierarchical porous $MnCo_2O_4$ microspheres through solvothermal method, which can deliver initial discharge capacity of 1034 mAh g^{-1} at a current density of 100 mA g^{-1} [33]. Chen and co-workers synthesized $MnCo_2O_4$/graphene sheets by hydrothermal method. Possessing a large surface area, the resulting material showed an initial discharge and charge capacity of 1350.4 and 962.5 mAh g^{-1} at a current density of 100 mA g^{-1}, respectively [34].

Several parameters such as anode compositions and morphology, slurry preparation and electrode fabrication process affect LIBs specific capacity, energy, power and cycle life performance. A key culprit in limiting the performance of lithium-ion batteries is insufficient conductivity, both electronic and ionic [35, 36].

The first discharge capacity is mainly determined by the electrochemical activity of the electrode as well as the kinetics of the device [37]. In particular, various parameters have been investigated for improving first discharge capacity. Adjustments in form factor [38], anode particle size and morphology [39, 40], anode particle arrangement [41], crystallinity index [42], porosity and thickness (active material loading) of the anode electrode [43] have all been shown to improve first discharge capacity.

The $MnCo_2O_4$ has been prepared by several synthesis techniques, however, no reports in the literature to explore a study on the effect of electrode preparation parameters on initial discharge capacity of $MnCo_2O_4$, so far. In this work, cubic spinel $MnCo_2O_4$ nanostructures are prepared via co-precipitation. To consider the influence of calcination temperature on initial discharge capacity, the precursor was calcined at 650 and 750°C. Anode laminates of various thicknesses and calendaring forces were prepared with the same chemical composition. The effects of calendaring (porosity) and electrode thickness (active material loading) on the initial discharge capacity were examined by discussing electrode conductivity.

2. Materials and Methods

2.1 Synthesis of $MnCo_2O_4$

Manganese cobaltite was synthesized via co-precipitation route. First, $Co(NO_3)_2.6H_2O$ (98%, Merck, Germany) and $Mn(NO_3)_2.4H_2O$ (99%, Merck, Germany) were dissolved in deionized water. Considering the molar ratio of 1.5, the aqueous solution of sodium hydroxide (NaOH) was added dropwise to the solution of metal nitrates with the rate of 10 ml/min at room temperature to obtain PH=13. The as-obtained brown precipitates were then filtered, washed with deionized water, and dried at 80°C for 18 h. Nanoparticles of $MnCo_2O_4$ were obtained by calcining the dried powder at 650 and 750°C for 5 h in air.

2.2 Powder characterization

The structure and phase purities of the products were characterized by X-ray diffraction (Rigaku Ultima IV) equipped with Cu target (Kα, λ =0.15406 nm). Particle size and morphology was assessed by a field-emission scanning electron microscope (FESEM) (TESCAN MIRA3). Thermogravimetric analysis (TGA) and differential thermal analysis (DTA) was done by LINSEIS L70/2171 with a heating rate of 5°C·min^{-1} from 40 to 900°C.

2.3 Electrochemical Measurements

The electrochemical tests were conducted using CR2032 coin cells. To fabricate anodes, a slurry was prepared by mixing super P carbon (10%), polyvinylidene fluoride (PVDF) binder (10%) and $MnCo_2O_4$ active material (80%). The adopted recipe included an optimized amount of n-methyl pyrrolidone (NMP) solvent achieved in our previous research [44]. To obtain anodes of different thicknesses, home-made automated doctor blade spreader was used for coating the slurry on a Cu foil with 12μm thickness. The electrode dried overnight in a conventional oven at 80°C and then in a vacuum oven for 2 h at 90°C. The coated films

were punched into discs of 14 mm diameters and then calendared at various forces (2900 N, 4850 N and 9700 N). The active material loading in the composite electrode ranged from 3-5 mg. In order to illustrate the effect of calendaring, the porosity of the electrode was calculated according to the equation 1 [45].

$$\text{Porosity} = \frac{L - W\left(\left(\frac{C1}{D1}\right) + \left(\frac{C2}{D2}\right) + \left(\frac{C3}{D3}\right)\right)}{L} \quad \text{(eq. 1)}$$

L: real electrode laminate thickness (without Cu foil)

W: weight of the laminate per area

C1, C2 and C3: percentage of active material, PVDF binder and super P

D1, D2 and D3: true density of active material (5.56 g cm^{-3}), PVDF binder (1.75 g cm^{-3}) and Super P (0.16 g.cm^{-3})

The coin cells were assembled in an Argon field glove box maintaining <1ppm of H_2O and O_2. Li metal (Gelon Co.) was used as the counter electrode. Solution of $LiPF_6$ (1 M) in ethyl carbonate -dimethyl carbonate (1:1 by volume) was employed as the electrolyte. Electrodes were separated by a microporous polyethylene film (Celgard 2400). The galvanostatic discharge-charge characteristics were measured in the range of 0.01 and 3.0 V using a Neware battery tester.

3. Results & Discussion

3.1 Thermal analysis

In order to obtain proper calcination conditions, TGA/DTA analysis was performed. Fig. 1 indicates thermal decomposition pattern of the precipitate in air atmosphere. The endothermic peak in the range of 60-150°C with a weight loss of 2% corresponds to the loss of absorbed and occluded water [46]. By increasing temperature up to 270°C, a change in slope of TGA curve in the range of 150-270°C with weight loss of about 9% is observed, which corresponds to the complete decomposition of the precipitate, complex precursor and metal nitrate. Although the 270°C exothermic peak, which is attributed to crystallization of $MnCo_2O_4$ phase, is not obvious in DTA curve (Fig. 1(a)), it could be clearly observed in Derivative differential thermal analysis (DDTA) results (Fig. 1(b)). No distinguished weight loss observed above 270°C. As a conclusion, formation of $MnCo_2O_4$ spinel oxide starts around 270°C and the structure is stable at least up to 900°C.

3.2 Structural studies

Fig. 2 indicates XRD patterns of calcined $MnCo_2O_4$ powder at 650 and 750°C. The diffraction peaks reveal the cubic spinel structure (JCPDS card no.23-1237) having Fd-3m (227) space group; The diffraction peaks at 2θ = 18.77°, 30.78°, 36.16°, 37.81°, 43.88°, 54.47°, 58.06°, 63.79°, 67.09°, 72.49°, 75.48° and 76.49° respectively correspond to (111), (220), (311), (222), (400), (422), (511), (440), (531), (620), (533) and (622) planes. No obvious impurity peaks are found, which indicates high purity of the as-synthesized samples. According to Scherrer equation [47] and based on XRD data, the average crystallite size of $MnCo_2O_4$ at two different temperatures of 650 and 750°C were calculated to be 18 and 23 nm, respectively; thus showing larger crystallite size with augmentation of the calcination temperature. Lower intensities and broader peaks of the sample calcined at 650°C indicates poor crystallinity compared to the one calcined in 750°C.

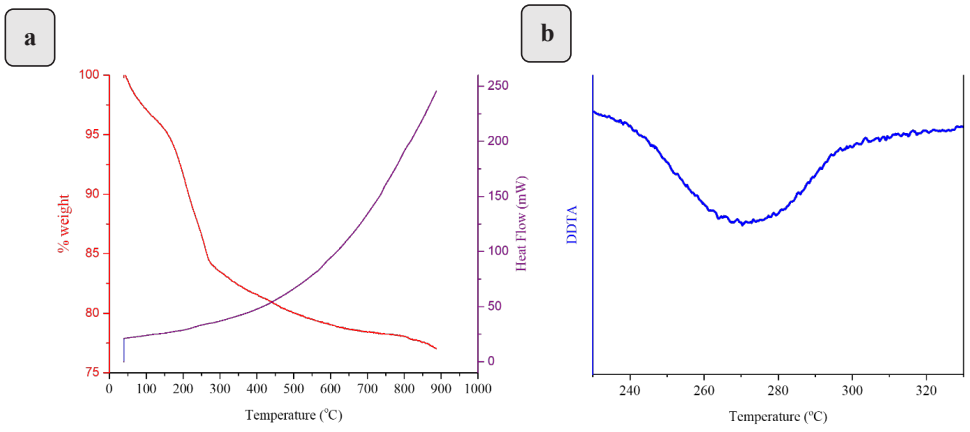

Fig. 1- (a) TGA/DTA (b) DDTA curves of the dried precipitates.

3.3 Morphology of $MnCo_2O_4$ powder

The FESEM images of $MnCo_2O_4$ powders calcined at 650 and 750°C are shown in Fig.3 (a) and (b) respectively. The material calcined at 650°C, exhibits quasi-plate particles with mean diameter of 105 nm and thickness of 24 nm. By increasing the calcination temperature to 750°C, morphology of the particles gradually changes to polyhedral with the mean size of 115 nm as shown in Fig.2 (b).

Previous studies illustrated that the presence of smaller particles, results in high porosity and relatively large specific surface area that offer immense electrolyte/materials contact area and enhance Li^+ diffusion, meanwhile the amorphous electrode materials bring faster reaction kinetics. Therefore, Confirming to previous reports, the calcined samples at 650°C is expected to exhibit better electrochemical performance due to smaller particles and lower crystallinity, which will be further discussed [42].

3.4 Electrochemical evaluation

Fig. 4 to 6 (obtained from galvanostatic cycling at a current density of 45 mA g^{-1}(C/20)), indicate initial specific discharge capacity of the samples fabricated under different conditions. Obviously, the initial specific discharge capacity of all samples are much higher than the theoretical capacity of $MnCo_2O_4$ (906 mAh g^{-1}) with the maximum of 1438 mAh g^{-1}. Similar behavior has also been observed in transition metal oxides such as Cobalt oxide [48], Nickel oxide [49], Manganese oxide

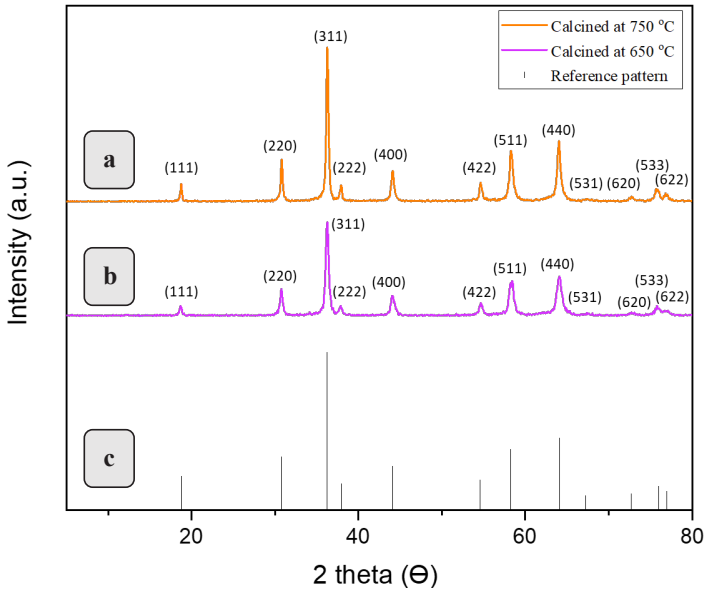

Fig. 2- The XRD patterns of powder calcined at (a) 750°C, (b) 650°C and (c) Reference pattern.

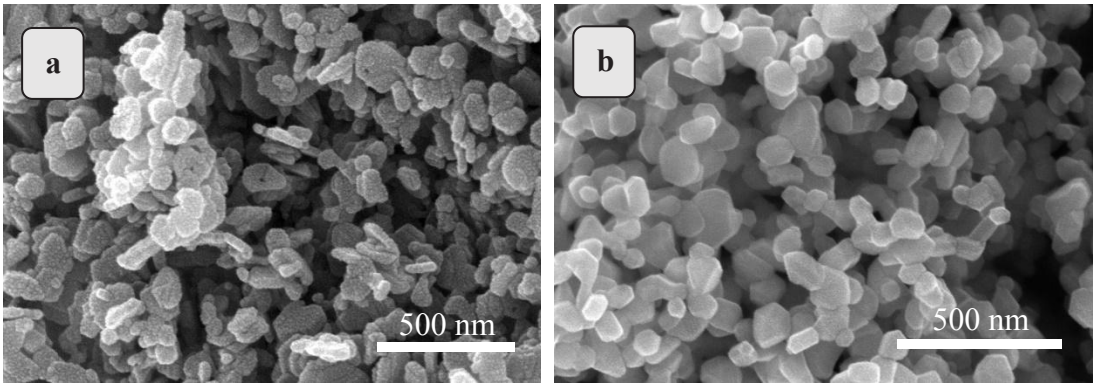

Fig. 3- FESEM image of powders calcined at (a) 650°C, (b) 750°C.

[50] and Iron oxide [51]. Although the reason of such a phenomenon is unclear, a plausible explanation is that the decomposition of electrolyte and the formation of solid electrolyte interphase (SEI) will lead to consumption of excess number of Li^+ ions. The SEI layer makes the initial Coulombic efficiency (54.34%) lower than its subsequent value (97.52%).

Fig. 4 discloses the calcination temperature effects on the initial specific discharge capacity of $MnCo_2O_4$ anode. In Fig. 4 (a) the thickness is 150 µm and two calendaring forces of 4850 and 9700 N are applied, while in Fig. 4 (b) the thickness is increased to 250 µm (same forces). The powder calcined at 650°C shows higher specific capacity in all test conditions which proves the strong effect of $MnCo_2O_4$ particles' inherent properties. According to the higher surface area (due to smaller particles) and weaker crystallinity, enhancement in electrode kinetic is concluded from XRD patterns and FESEM images.

Changes of the initial specific discharge capacity of $MnCo_2O_4$ active materials sintered at 650°C in different porosity for three constant thicknesses is illustrated in fig. 5. It is clearly observed that the initial specific discharge capacity increased with decreasing porosity in all different thicknesses.

Notably, decrease in electrode porosity has two conflicting achievements; electrode layer compression and particle-to-particle contact increase, which improves electronic conductivity. On the other hand, as explained by Zheng et al [52], applying pressure on electrode turns open pores to closed ones. Following it, the wettability

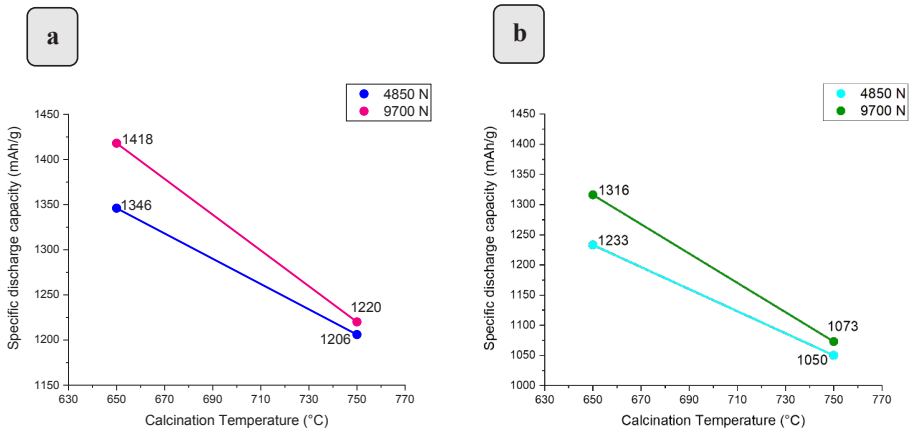

Fig. 4- Initial discharge capacity as a function of calcination temperature at two applied calendaring forces (4850 and 9700 N), (a) thickness of 150 µm (b) thickness of 250 µm.

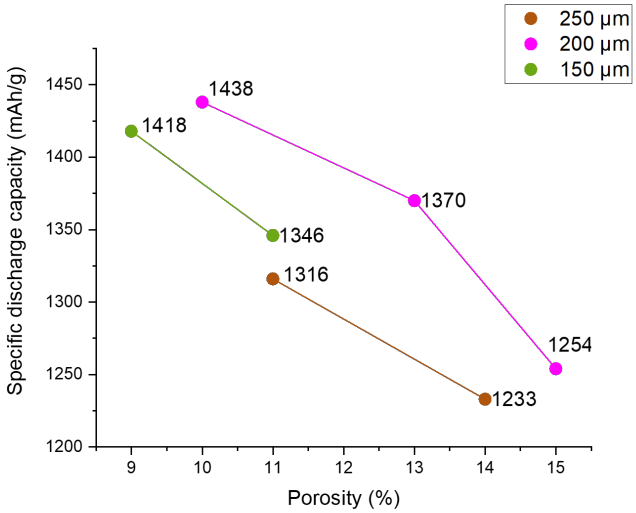

Fig. 5- Initial discharge capacity as a function of porosities at different thicknesses for the $MnCo_2O_4$ calcined at 650°C.

of electrode with electrolyte decreases. Therefore, the active material may not get wet with electrolyte and would be electrochemically inert during discharge-charge cycles resulting in lower the electronic conductivity. Considering low electronic conductivity of the electrode studied in this work, an increase of particle-to-particle contact compensates the negative effect of wettability reduction. Thus, the higher specific discharge capacity is achieved [53].

Fig. 6 shows the capacities of $MnCo_2O_4$ active material calcined at 650°C, obtained at constant calendaring forces in different laminate thicknesses. Fig 6 indicates that the specific discharge capacity decreases with thickness increment. A slight increase is observed when the electrode thickness increases from 150 to 200 µm which is ignorable. To justify the thickness effect on specific discharge capacity, the electrode was considered as a compound consisting of two phases: (1) liquid electrolyte within the pores and (2) the porous solid matrices. The decrease in capacity of the anodes depends on several transport phenomena such as: (1) Li ions' diffusion through the solid electrolyte interphase (SEI) film, R_{SEI}; (2) Li ions' diffusion within the bulk electrode, R_{diff}; (3) transport of Li ions in the electrolyte towards the active material surface, R_s; (4) Electronic resistance of the electrode, R_e; (5) Li ions charge transfer at the electrode/electrolyte interface, R_{ct}.

The electronic resistance of the electrode can be calculated from $R_e = L/\sigma$, where L is the thickness

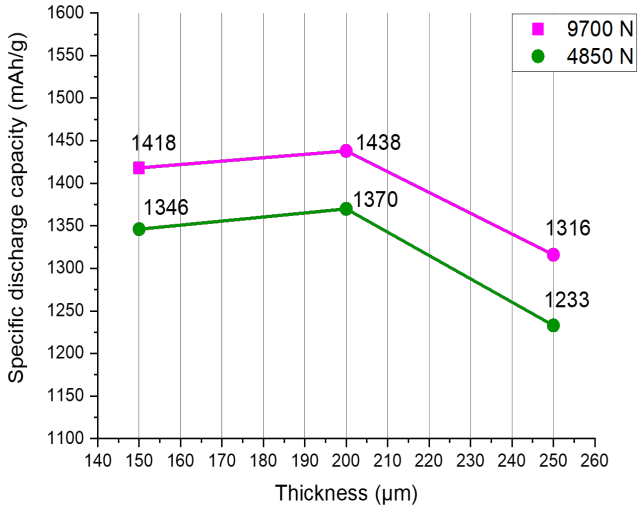

Fig. 6- Initial discharge capacity as a function of thickness at different calendaring forces for the $MnCo_2O_4$ calcined at 650°C.

Table 1-Comparison of the important MCO complex oxides electrochemical performance between this work and the previous reports

Complex oxide	Initial Discharge capacity ($mAh.g^{-1}$)	Current density ($mA.g^{-1}$)	Ref.
$MnCo_2O_4$ quasi-plate	1438	45	This work
$MnCo_2O_4$ quasi-hollow microsphere	1473	200	[1]
$MnCo_2O_4$ hierarchical porous microspheres	1034	1000	[2]
$MnCo_2O_4$ nanoparticles	1200	100	[3]
$MnCo_2O_4$ flake-like	1460	100	[4]
$MnCo_2O_4$ nanospheres	1184	400	[56]
Hollow $MnCo_2O_4$ Submicrospheres	1425	400	[57]

and σ represents electronic conductivity of the electrode layer. The increase of L obviously leads to electronic resistance rise of the electrode [54].

A comparison between the manganese cobaltite reported in literature and our product is summarized in Table 1. Obviously, the as-synthesized quasi-plate $MnCo_2O_4$ exhibits good electrochemical performance.

4. Conclusions

In summary, nanostructured manganese cobalt oxide ($MnCo_2O_4$) was successfully synthesized by co-precipitation method. Results of thermal analysis indicated that crystallization of $MnCo_2O_4$ started at 270°C which remains stable at higher temperatures because no prominent weight loss was observed. It is important to optimize the thermal annealing temperature for best electrochemical performance. $MnCo_2O_4$ powders calcined at 650°C show higher initial discharge capacity in all electrode preparation conditions, as a result of relatively lower crystallinity and higher surface area. The electrode conductivity of the laminates depends strongly on their thickness and porosity. Changes in these two parameters lead to initial capacity change.

Acknowledgments

The authors would like to acknowledge the Advanced Materials Characterization Institute (AMCI), University of Tehran and Iran Nanotechnology Initiative Council for their financial supports.

References

1. Goodenough JB, Kim Y. Challenges for Rechargeable Li Batteries†. Chemistry of Materials. 2010;22(3):587-603.
2. Liu S, Hui KS, Hui KN. Back Cover: 1D Hierarchical MnCo2O4Nanowire@MnO2Sheet Core-Shell Arrays on Graphite Paper as Superior Electrodes for Asymmetric Supercapacitors (ChemNanoMat 8/2015). ChemNanoMat. 2015;1(8):616-.
3. Etacheri V, Marom R, Elazari R, Salitra G, Aurbach D. Challenges in the development of advanced Li-ion batteries: a review. Energy & Environmental Science. 2011;4(9):3243.
4. Yuan L-X, Wang Z-H, Zhang W-X, Hu X-L, Chen J-T, Huang Y-H, et al. Development and challenges of LiFePO4cathode material for lithium-ion batteries. Energy Environ Sci. 2011;4(2):269-84.
5. Mondal AK, Su D, Chen S, Ung A, Kim H-S, Wang G. Mesoporous MnCo2O4with a Flake-Like Structure as Advanced Electrode Materials for Lithium-Ion Batteries and Supercapacitors. Chemistry - A European Journal. 2014;21(4):1526-32.
6. Winter M, Besenhard JO, Spahr ME, Novák P. Insertion Electrode Materials for Rechargeable Lithium Batteries. Advanced Materials. 1998;10(10):725-63.
7. Poizot P, Laruelle S, Grugeon S, Dupont L, Tarascon JM. Nano-sized transition-metal oxides as negative-electrode materials for lithium-ion batteries. Nature. 2000;407(6803):496-9.
8. Reddy MV, Xu Y, Rajarajan V, Ouyang T, Chowdari BVR. Template Free Facile Molten Synthesis and Energy Storage Studies on MCo2O4 (M = Mg, Mn) as Anode for Li-Ion Batteries. ACS Sustainable Chemistry & Engineering. 2015;3(12):3035-42.
9. Liu H, Bi Z, Sun X-G, Unocic RR, Paranthaman MP, Dai S, et al. Mesoporous TiO2-B Microspheres with Superior Rate Performance for Lithium Ion Batteries. Advanced Materials. 2011;23(30):3450-4.
10. Rajagopalan B, Oh ES, Chung JS. The effect of diethylenetriamine on the solvothermal reactions of polyethyleneimine-graphene oxide/lithium titanate nanocomposites for lithium battery anode. Journal of Power Sources. 2015;275:702-11.
11. Sun C, Li F, Ma C, Wang Y, Ren Y, Yang W, et al. Graphene–Co3O4 nanocomposite as an efficient bifunctional catalyst for lithium–air batteries. J Mater Chem A. 2014;2(20):7188-96.
12. Feng X, Liang Y, Zhi L, Thomas A, Wu D, Lieberwirth I, et al. Synthesis of Microporous Carbon Nanofibers and Nanotubes from Conjugated Polymer Network and Evaluation in Electrochemical Capacitor. Advanced Functional Materials. 2009;19(13):2125-9.
13. An G-H, Ahn H-J. Carbon nanofiber/cobalt oxide nanopyramid core–shell nanowires for high-performance lithium-ion batteries. Journal of Power Sources. 2014;272:828-36.
14. Jin Y, Wang L, Shang Y, Gao J, Li J, He X. Facile synthesis of monodisperse Co3O4 mesoporous microdisks as an anode material for lithium ion batteries. Electrochimica Acta. 2015;151:109-17.
15. Xu Y, Wang X, An C, Wang Y, Jiao L, Yuan H. Effect of the length and surface area on electrochemical performance of cobalt oxide nanowires for alkaline secondary battery application. Journal of Power Sources. 2014;272:703-10.
16. Zhang J, Huang T, Yu A. Synthesis and effect of electrode heat-treatment on the superior lithium storage performance of Co 3 O 4 nanoparticles. Journal of Power Sources. 2015;273:894-903.
17. Cheng JP, Chen X, Wu J-S, Liu F, Zhang XB, Dravid VP. Porous cobalt oxides with tunable hierarchical morphologies for supercapacitor electrodes. CrystEngComm. 2012;14(20):6702.
18. Wang K, Liu G, Hoivik N, Johannessen E, Jakobsen H. Electrochemical engineering of hollow nanoarchitectures: pulse/step anodization (Si, Al, Ti) and their applications. Chem Soc Rev. 2014;43(5):1476-500.
19. Yang Z, Yao Z, Li G, Fang G, Nie H, Liu Z, et al. Sulfur-Doped Graphene as an Efficient Metal-free Cathode Catalyst for Oxygen Reduction. ACS Nano. 2011;6(1):205-11.
20. Brun N, Sakaushi K, Yu L, Giebeler L, Eckert J, Titirici MM. Hydrothermal carbon-based nanostructured hollow spheres as electrode materials for high-power lithium–sulfur batteries. Physical Chemistry Chemical Physics. 2013;15(16):6080.
21. Datta MK, Maranchi J, Chung SJ, Epur R, Kadakia K, Jampani P, et al. Amorphous silicon–carbon based nano-scale thin film anode materials for lithium ion batteries. Electrochimica Acta. 2011;56(13):4717-23.
22. Wang L, Yu Y, Chen PC, Zhang DW, Chen CH. Electrospinning synthesis of C/Fe3O4 composite nanofibers and their application for high performance lithium-ion batteries. Journal of Power Sources. 2008;183(2):717-23.
23. Wang Z, Zhou L, David Lou XW. Metal Oxide Hollow Nanostructures for Lithium-ion Batteries. Advanced Materials. 2012;24(14):1903-11.
24. Reddy MV, Kenrick KYH, Wei TY, Chong GY, Leong GH, Chowdari BVR. Nano-ZnCo2O4 Material Preparation by Molten Salt Method and Its Electrochemical Properties for Lithium Batteries. Journal of The Electrochemical Society. 2011;158(12):A1423.
25. Reddy MV, Yu C, Jiahuan F, Loh KP, Chowdari BVR. Molten salt synthesis and energy storage studies on CuCo2O4 and

CuO·Co3O4. RSC Advances. 2012;2(25):9619.
26. Sharma Y, Sharma N, Subbarao G, Chowdari B. Studies on spinel cobaltites, FeCo2O4 and MgCo2O4 as anodes for Li-ion batteries. Solid State Ionics. 2008;179(15-16):587-97.
27. Cherian CT, Sundaramurthy J, Reddy MV, Suresh Kumar P, Mani K, Pliszka D, et al. Morphologically Robust NiFe2O4 Nanofibers as High Capacity Li-Ion Battery Anode Material. ACS Applied Materials & Interfaces. 2013;5(20):9957-63.
28. Hameed AS, Bahiraei H, Reddy MV, Shoushtari MZ, Vittal JJ, Ong CK, et al. Lithium Storage Properties of Pristine and (Mg, Cu) Codoped ZnFe2O4 Nanoparticles. ACS Applied Materials & Interfaces. 2014;6(13):10744-53.
29. Reddy MV, Quan CY, Teo KW, Ho LJ, Chowdari BVR. Mixed Oxides, (Ni1–xZnx)Fe2O4 (x = 0, 0.25, 0.5, 0.75, 1): Molten Salt Synthesis, Characterization and Its Lithium-Storage Performance for Lithium Ion Batteries. The Journal of Physical Chemistry C. 2015;119(9):4709-18.
30. Zhao J, Yang B, Zheng Z, Yang J, Yang Z, Zhang P, et al. Facile Preparation of One-Dimensional Wrapping Structure: Graphene Nanoscroll-Wrapped of Fe3O4 Nanoparticles and Its Application for Lithium-Ion Battery. ACS Applied Materials & Interfaces. 2014;6(12):9890-6.
31. Yu L, Zhang L, Wu HB, Zhang G, Lou XW. Controlled synthesis of hierarchical CoxMn3–xO4array micro-/nanostructures with tunable morphology and composition as integrated electrodes for lithium-ion batteries. Energy Environ Sci. 2013;6(9):2664-71.
32. Hwang SM, Kim SY, Kim J-G, Kim KJ, Lee J-W, Park M-S, et al. Electrospun manganese–cobalt oxide hollow nanofibres synthesized via combustion reactions and their lithium storage performance. Nanoscale. 2015;7(18):8351-5.
33. Li G, Xu L, Zhai Y, Hou Y. Fabrication of hierarchical porous MnCo2O4 and CoMn2O4 microspheres composed of polyhedral nanoparticles as promising anodes for long-life LIBs. Journal of Materials Chemistry A. 2015;3(27):14298-306.
34. Chen C, Liu B, Ru Q, Ma S, An B, Hou X, et al. Fabrication of cubic spinel MnCo 2 O 4 nanoparticles embedded in graphene sheets with their improved lithium-ion and sodium-ion storage properties. Journal of Power Sources. 2016;326:252-63.
35. Liu Z, Battaglia V, Mukherjee PP. Mesoscale Elucidation of the Influence of Mixing Sequence in Electrode Processing. Langmuir. 2014;30(50):15102-13.
36. Myung S-T, Cho MH, Hong HT, Kang TH, Kim C-S. Electrochemical evaluation of mixed oxide electrode for Li-ion secondary batteries: Li1.1Mn1.9O4 and LiNi0.8Co0.15Al0.05O2. Journal of Power Sources. 2005;146(1-2):222-5.
37. Etacheri V, Yourey JE, Bartlett BM. Chemically Bonded TiO2–Bronze Nanosheet/Reduced Graphene Oxide Hybrid for High-Power Lithium Ion Batteries. ACS Nano. 2014;8(2):1491-9.
38. Thomas KE, Sloop SE, Kerr JB, Newman J. Comparison of lithium-polymer cell performance with unity and nonunity transference numbers. Journal of Power Sources. 2000;89(2):132-8.
39. Chen YH, Wang CW, Zhang X, Sastry AM. Porous cathode optimization for lithium cells: Ionic and electronic conductivity, capacity, and selection of materials. Journal of Power Sources. 2010;195(9):2851-62.
40. Sheu SP, Yao CY, Chen JM, Chiou YC. Influence of the LiCoO2 particle size on the performance of lithium-ion batteries. Journal of Power Sources. 1997;68(2):533-5.
41. Wang C-W, Sastry AM. Mesoscale Modeling of a Li-Ion Polymer Cell. Journal of The Electrochemical Society. 2007;154(11):A1035.
42. Jiang Y, Zhang D, Li Y, Yuan T, Bahlawane N, Liang C, et al. Amorphous Fe2O3 as a high-capacity, high-rate and long-life anode material for lithium ion batteries. Nano Energy. 2014;4:23-30.
43. Srinivasan V, Newman J. Design and Optimization of a Natural Graphite/Iron Phosphate Lithium-Ion Cell. Journal of The Electrochemical Society. 2004;151(10):A1530.
44. Dorri M, Zamani C, Babaei A. An investigation on the effect of deposition parameters on nanostructured electrode of lithium ion batteries and their performance. Author(s); 2018.
45. Liu G, Zheng H, Kim S, Deng Y, Minor AM, Song X, et al. Effects of Various Conductive Additive and Polymeric Binder Contents on the Performance of a Lithium-Ion Composite Cathode. Journal of The Electrochemical Society. 2008;155(12):A887.
46. Padmanathan N, Selladurai S. Mesoporous MnCo2O4 spinel oxide nanostructure synthesized by solvothermal technique for supercapacitor. Ionics. 2013;20(4):479-87.
47. Wilson AJC. Elements of X-ray Diffraction by B. D. Cullity. Acta Crystallographica. 1957;10(1):88-.
48. Jadhav HS, Rai AK, Lee JY, Kim J, Park C-J. Enhanced electrochemical performance of flower-like Co 3 O 4 as an anode material for high performance lithium-ion batteries. Electrochimica Acta. 2014;146:270-7.
49. Liu W, Lu C, Wang X, Liang K, Tay BK. In situ fabrication of three-dimensional, ultrathin graphite/carbon nanotube/NiO composite as binder-free electrode for high-performance energy storage. Journal of Materials Chemistry A. 2015;3(2):624-33.
50. Yue J, Gu X, Chen L, Wang N, Jiang X, Xu H, et al. General synthesis of hollow MnO2, Mn3O4and MnO nanospheres as superior anode materials for lithium ion batteries. J Mater Chem A. 2014;2(41):17421-6.
51. Zhu X, Song X, Ma X, Ning G. Enhanced Electrode Performance of Fe2O3 Nanoparticle-Decorated Nanomesh Graphene As Anodes for Lithium-Ion Batteries. ACS Applied Materials & Interfaces. 2014;6(10):7189-97.
52. Zheng H, Liu G, Song X, Ridgway P, Xun S, Battaglia VS. Cathode Performance as a Function of Inactive Material and Void Fractions. Journal of The Electrochemical Society. 2010;157(10):A1060.
53. Zheng H, Tan L, Liu G, Song X, Battaglia VS. Calendering effects on the physical and electrochemical properties of Li[Ni1/3Mn1/3Co1/3]O2 cathode. Journal of Power Sources. 2012;208:52-7.
54. Zheng H, Li J, Song X, Liu G, Battaglia VS. A comprehensive understanding of electrode thickness effects on the electrochemical performances of Li-ion battery cathodes. Electrochimica Acta. 2012;71:258-65.
55. Li J, Xiong S, Li X, Qian Y. A facile route to synthesize multiporous MnCo2O4 and CoMn2O4 spinel quasi-hollow spheres with improved lithium storage properties. Nanoscale. 2013;5(5):2045.
56. Zhou S, Luo X, Chen L, Xu C, Yan D. MnCo2O4 nanospheres for improved lithium storage performance. Ceramics International. 2018;44(15):17858-63.
57. Li J, Wang J, Liang X, Zhang Z, Liu H, Qian Y, et al. Hollow MnCo2O4 Submicrospheres with Multilevel Interiors: From Mesoporous Spheres to Yolk-in-Double-Shell Structures. ACS Applied Materials & Interfaces. 2013;6(1):24-30.